 © 2007 The Chemical Society of Japan

Selected Paper

Syntheses and Crystal Structures of Mono(di-2-pyridylamine)chloro-(dimethyl sulfoxide-*S*)ruthenium(II) Complexes $[RuCl_2(Hdpa)(dmso\text{-}S)_2]$ and $[RuCl(Hdpa)(dmso\text{-}O)(dmso\text{-}S)_2](OTf)$

Mari Toyama,* Ryuji Suganoya, Daisuke Tsuduura, and Noriharu Nagao*

Department of Applied Chemistry, Meiji University, Kawasaki 214-8571

Received September 28, 2006; E-mail: nori@isc.meiji.ac.jp

The reaction between *trans*-$[RuCl_2(dmso\text{-}S)_4]$ (dmso = dimethyl sulfoxide) and di-2-pyridylamine (Hdpa) in EtOH–H_2O at ca. 273 K afforded *trans*(Cl),*cis*(S)-$[RuCl_2(Hdpa)(dmso\text{-}S)_2]$ (**1**) in moderate to high yield. When dissolved in DMSO, **1** rearranged to the more thermodynamically stable *cis*(Cl),*cis*(S)-$[RuCl_2(Hdpa)(dmso\text{-}S)_2]$ (**2**), along with *cis*(Cl),*trans*(X)-$[RuCl_2(Hdpa)(dmso)_2]$ (X = *S*- or *O*-bonded dmso). The reaction of **2** with Ag(OTf) afforded *cis*(Cl,S),*trans*(O,S)-$[RuCl(Hdpa)(dmso\text{-}O)(dmso\text{-}S)_2](OTf)$ (**3•(OTf)**) (OTf^- = trifluoromethanesulfonate). X-ray crystal structures of **1**, **2**, and **3•(OTf)** revealed that the conformation of the six-membered chelate ring formed by the Hdpa ligand with the Ru ion varies according to interactions among the co-ligands (dmso and Cl^-) and the counter-anion (OTf^-). For **3•(OTf)**, the structural parameters, apart from the dmso-*O* ligand, were essentially comparable to those of **2**, except for the axial Cl^- ligand; the remaining axial site is occupied by the *O*-donor of the dmso ligand instead of the *S*-donor. The solution structures (in DMSO solution) of **1**, **2**, and **3•(OTf)** are discussed on the basis of their ^1H NMR spectra. In **3•(OTf)**, "flapping" of the Hdpa ligand causes the coordination modes (*O*- and *S*-bonded) of the two axial dmso ligands to undergo mutual alternation.

Ruthenium(II) complexes containing polypyridyl ligands have been the subject of much interest due to their photochemical, electrochemical, and biochemical properties.[1–10] Most of the ruthenium(II) polypyridyl complexes that have hitherto been investigated are homoleptic or bis-heteroleptic polypyridyl ruthenium(II) complexes, because it is difficult to synthesize the precursor mono(polypyridyl)ruthenium(II) complex required for the preparation of tris-heteroleptic polypyridyl ruthenium(II) complexes. Various strategies have been proposed and carried out to obtain mono(polypyridyl)ruthenium(II) complexes with 2,2′-bipyridine (bpy), 1,10-phenanthroline (phen), or analogous ligands, which form a five-membered chelate ring with a metal ion.[11–23]

We have previously reported the selective syntheses and crystal structures of *trans*(Cl),*cis*(S)- and *cis*(Cl),*cis*(S)-$[RuCl_2(bpy)(dmso\text{-}S)_2]$.[24] Although a third, i.e., *cis*(Cl),*trans*(S)-isomer has not been isolated, its geometry was verified using X-ray crystallography. In our synthesis, *trans*-$[RuCl_2(dmso\text{-}S)_4]$, which has been synthesized and characterized by Alessio and co-workers,[25,26] is used as the starting material, rather than the conventional *cis*(Cl),*fac*(S)-$[RuCl_2(dmso\text{-}S)_3(dmso\text{-}O)]$. The reaction between *trans*-$[RuCl_2(dmso\text{-}S)_4]$ and bpy in EtOH–H_2O at 273 K affords the *trans*(Cl),*cis*(S)-isomer in good yield. When dissolved in DMSO, the *trans*(Cl),*cis*(S)-isomer rearranges to the more thermodynamically stable *cis*(Cl),*cis*(S)-isomer, along with a small amount of a third *cis*(Cl),*trans*(S)-isomer. The *cis*(Cl),*cis*(S)-isomer can be selectively synthesized by heating the *trans*(Cl),*cis*(S)-isomer in EtOH–DMSO (9:1). The three isomers isomerize in DMSO solution. In contrast to the reversible isomerization between the *cis*(Cl),*cis*(S)-isomer and the *cis*(Cl),*trans*(S)-isomer, isomerization from the *trans*(Cl),*cis*(S)-isomer to the *cis*(Cl),*cis*(S)-isomer is irreversible. Furthermore, our studies have shown that intramolecular non-classical hydrogen bonding, such as CH···O and CH···Cl–Ru interactions, between the bpy and dmso or Cl^- ligands or between two dmso ligands may explain the distortion, stability, and special features of the mono(2,2′-bipyridine)-ruthenium(II) complexes $[RuCl_2(bpy)(dmso\text{-}S)_2]$.[24]

Di-2-pyridylamine (Hdpa) has been widely used as a polypyridyl ligand in a variety of metal complexes.[11–14,27–38] Hdpa, which is an analogue of the bpy ligand, most commonly coordinates through both of its pyridyl nitrogen atoms. However, while the bpy ligand forms a rigid five-membered chelate ring, the Hdpa ligand forms a non-planar flexible six-membered chelate ring. A number of ruthenium complexes with Hdpa are heteroleptic with another polypyridyl ligand (bpy and phen).[11–14,33–35] There are only four reports concerning mono-(di-2-pyridylamine)ruthenium(II) complexes without other polypyridyl ligands, and as far as we know, all of these are about $[RuCl_2(Hdpa)(CO)_2]$.[36–39] Haukka and co-workers reported that $[RuCl_2(Hdpa)(CO)_2]$ is obtained from the reaction between $Ru_3(CO)_{12}$ and Hdpa and from the reaction of $RuCl_3$ with Hdpa under a CO atmosphere.[36] These methods give a mixture of geometrical isomers, *trans*(Cl),*cis*(CO)- and *cis*(Cl),*cis*(CO)-$[RuCl_2(Hdpa)(CO)_2]$, and the *cis*(Cl),*cis*(CO)-isomer has been characterized by single crystal X-ray crystallography. Although the reaction between $[\{RuCl_2(CO)_3\}_2]$ and Hdpa selectively produces the *trans*(Cl),*cis*(CO)-isomer, the total yield is very low (5%).

With the aim of increasing the range of ligands that can be

Published on the web May 14, 2007; doi:10.1246/bcsj.80.922

adapted to our synthetic method, we report in this paper the selective syntheses and crystal structures of *trans*(Cl),*cis*(S)- and *cis*(Cl),*cis*(S)-[$RuCl_2$(Hdpa)(dmso-*S*)$_2$] (**1** and **2**, respectively). They were synthesized according to the methods used for *trans*(Cl),*cis*(S)- and *cis*(Cl),*cis*(S)-[$RuCl_2$(bpy)(dmso-*S*)$_2$].[24] Furthermore, the synthesis and crystal structure of *cis*(Cl,S),-*trans*(O,S)-[RuCl(Hdpa)(dmso-*O*)(dmso-*S*)$_2$](OTf) (**3•(OTf)**) (OTf^- = trifluoromethanesulfonate), which was afforded by the reaction between **2** and Ag(OTf) in DMSO solution, is also reported.

Experimental

Hydrated ruthenium trichloride, $RuCl_3 \cdot 3H_2O$, was purchased from Furuya Kinzoku Co. All other solvents and chemicals were of reagent quality and were used without further purification. The starting materials *cis*(Cl),*fac*(S)-[$RuCl_2$(dmso-*S*)$_3$(dmso-*O*)] and *trans*-[$RuCl_2$(dmso-*S*)$_4$] were prepared according to literature methods.[22,25] Di-2-pyridylamine (Hdpa) ligand was prepared by a base-catalyzed coupling reaction of 2-aminopyridine and 2-chloropyridine (1:1 ratio).[40] Sodium hydride was used as a base, and THF was used as a solvent.[28] All reactions were carried out under an argon atmosphere.

Kinetic studies were performed on **1**, **2**, and **3•(OTf)** using ^{1}H NMR spectroscopy in DMSO-d_6; kinetic data was obtained from successive ^{1}H NMR spectra. The intensities of selected signals were normalized with respect to a reference signal (mesitylene) or set of signals (usually the sum of the intensities of the H-6 signals for all species).

Synthesis of *trans*(Cl),*cis*(S)-[$RuCl_2$(Hdpa)(dmso-*S*)$_2$]• 0.5EtOH (1•0.5EtOH). A suspension of *trans*-[$RuCl_2$(dmso-*S*)$_4$] (1.5 g, 3 mmol) and Hdpa (0.54 g, 3 mmol) in a mixture of EtOH (15 mL) and H_2O (15 mL) was allowed to stir for 40 h at ca. 273 K. With stirring, *trans*-[$RuCl_2$(dmso-*S*)$_4$] and Hdpa gradually dissolved (after ca. 0.5 h), and a yellow precipitate, *trans*(Cl),*cis*(S)-[$RuCl_2$(Hdpa)(dmso-*S*)$_2$] (**1**), slowly formed. This was collected by filtration, washed with cold EtOH, and dried in vacuo (1.3 g, 75%). Yellow crystals of **1•0.5EtOH** suitable for X-ray crystallography were obtained by vapor diffusion of diethyl ether into a mixed solution of EtOH and DMSO (40:1) of **1**. Anal. Calcd for $C_{14}H_{21}N_3Cl_2O_2S_2Ru \cdot 0.5(C_2H_5OH)$: C, 34.48; H, 4.63; N, 8.04%. Found: C, 34.35; H, 4.56; N, 8.06%. ^{1}H NMR (270 MHz, DMSO-d_6): δ 3.15 (12H, br s, CH_3 of dmso), 7.06 (4H, m, H-3 and H-5), 7.79 (2H, t, J = 7.7 Hz, H-4), 8.58 (2H, d, J = 5.0 Hz, H-6), 10.73 (1H, s, N-Ha).

Synthesis of *cis*(Cl),*cis*(S)-[$RuCl_2$(Hdpa)(dmso-*S*)$_2$] (2). A suspension of **1** (0.75 g, 1.5 mmol) in a mixture of EtOH (14 mL) and DMSO (1 mL) was refluxed for about 5 min. While refluxing, the suspension of yellow solid **1** became homogeneous (after about 2 min), followed by the gradual appearance of a yellow precipitate, *cis*(Cl),*cis*(S)-[$RuCl_2$(Hdpa)(dmso-*S*)$_2$] (**2**). The reaction mixture was cooled to room temperature, and EtOH (35 mL) was added to the reaction solution in a sufficient amount to precipitate the product. The yellow precipitate was collected by filtration, washed with EtOH, and dried in vacuo (0.55 g, 75%). Anal. Calcd for $C_{14}H_{21}N_3Cl_2O_2S_2Ru$: C, 33.66; H, 4.24; N, 8.41%. Found: C, 33.88; H, 4.21; N, 8.43%. ^{1}H NMR (270 MHz, DMSO-d_6): δ 2.66 (3H, s, CH_3 of dmso), 3.25 (3H, s, CH_3 of dmso), 3.26 (3H, s, CH_3 of dmso), 3.35 (3H, s, CH_3 of dmso), 6.83 (1H, dd, J = 6.2, 7.2 Hz, H-5′), 6.95 (1H, dd, J = 6.1, 7.1 Hz, H-5), 7.02 (1H, d, J = 8.5 Hz, H-3′), 7.07 (1H, d, J = 8.5 Hz, H-3), 7.72 (1H, dd, J = 7.0, 8.4 Hz, H-4′), 7.80 (1H, dd, J = 7.0, 8.4 Hz, H-4), 8.79 (1H, d, J = 6.2 Hz, H-6′), 8.97 (1H, d, J = 6.2 Hz, H-6), 10.57 (1H, s, N-Ha).

Yellow crystals of **2•0.85DMSO** suitable for X-ray crystallography were obtained by diffusion of EtOH and diethyl ether into a DMSO solution of **2**. During crystallization, DMSO (0.85 molecules) was incorporated into the unit cell of **2**. Anal. Calcd for $C_{14}H_{21}N_3Cl_2O_2S_2Ru \cdot 0.85(C_2H_6O_1S_1)$: C, 33.32; H, 4.65; N, 7.43%. Found: C, 33.38; H, 4.61; N, 7.26%.

Synthesis of *cis*(Cl,S),*trans*(O,S)-[RuCl(Hdpa)(dmso-*O*)-(dmso-*S*)$_2$](OTf) (3•(OTf)). A suspension of yellow solid **2** (0.50 g, 1.0 mmol) in DMSO (5 mL) was heated to 373 K for 10 min, during which the suspension became homogeneous. One equiv of Ag(OTf) (0.26 g, 1.0 mmol) was added, and the reaction mixture was heated for 5 min. The resulting AgCl precipitate was removed by filtration. After the filtrate was cooled to room temperature, EtOH (5 mL) and diethyl ether (50 mL) were added to the filtrate to precipitate the yellow product, *cis*(Cl,S),*trans*(O,S)-[RuCl(Hdpa)(dmso-*O*)(dmso-*S*)$_2$](OTf) (**3•(OTf)**). The product was washed several times by decantation with small amounts of diethyl ether. The yellow precipitate was then collected by filtration, washed with diethyl ether, and dried in vacuo (0.58 g, 83%). Yellow crystals of **3•(OTf)** suitable for X-ray crystallography were obtained by vapor diffusion of diethyl ether into a mixed EtOH–DMSO solution of **3•(OTf)**. Anal. Calcd for $C_{17}H_{27}N_3ClF_3O_6S_4Ru$: C, 29.54; H, 3.94; N, 6.08%. Found: C, 29.55; H, 3.87; N, 5.96%. ^{1}H NMR (270 MHz, DMSO-d_6): δ 2.61 (3H, s, CH_3 of dmso), 2.68 (3H, s, CH_3 of dmso), 2.72 (3H, s, CH_3 of dmso), 3.08 (3H, s, CH_3 of dmso), 3.36 (3H, s, CH_3 of dmso), 3.40 (3H, s, CH_3 of dmso), 6.97 (1H, dd, J = 7.7, 6.2 Hz, H-5), 7.14 (2H, m, H-3 and H-5′), 7.28 (1H, d, J = 7.9 Hz, H-3′), 7.83 (1H, t, J = 7.7 Hz, H-4), 7.98 (1H, t, J = 7.9 Hz, H-4′), 8.75 (1H, d, J = 6.1 Hz, H-6′), 8.83 (1H, d, J = 6.2 Hz, H-6), 10.80 (1H, s, N-Ha).

X-ray Crystallography. Data for all crystals were collected using the ω-2θ scan technique ($2\theta < 55^\circ$) on a Rigaku AFC-7R automated four-circle X-ray diffractometer with graphite-monochromatized Mo Kα radiation (λ = 0.71069 Å) at 296 K. All calculations were carried out on an O_2 workstation (SGI) using the teXsan crystallographic software package.[41] The structures were solved by the direct method and expanded using Fourier techniques. The non-hydrogen atoms were refined anisotropically. Hydrogen atoms were placed in idealized positions and included in the structure factor calculations. For **1**, the center of the C–C bond of an EtOH molecule was situated on a crystallographic center of symmetry, and the O atom of the EtOH was disordered over four positions with 0.25 occupancy factor. For **2**, disordered DMSO molecules (0.85 molecules) were included at general position, which was modeled by a three-site positional disorder. The hydrogen atoms of disordered solvent ethanol and DMSO were not included in the structure factor calculations. The crystallographic data for **1•0.5EtOH**, **2•0.85DMSO**, and **3•(OTf)** are summarized in Table 1. Selected bond lengths and angles are listed in Tables 2 and 3, respectively. Selected non-bonding contacts and angles are listed in Table S1.

Crystallographic data have been deposited with Cambridge Crystallographic Data Centre: deposition numbers CCDC-622241–622243 for compounds Nos. **1**, **2**, and **3•(OTf)**, respectively. Copies of the data can be obtained free of charge via http://www.ccdc.cam.ac.uk/conts/retrieving.html (or from the Cambridge Crystallographic Data Centre, 12, Union Road, Cambridge, CB2 1EZ, UK; Fax: +44 1223 336033, e-mail: deposit@ccdc.cam.ac.uk).

Table 1. Crystallographic Data for **1**, **2**, and **3·(OTf)**

	1·0.5EtOH	**2·0.85DMSO**	**3·(OTf)**
Experimental formula	$RuCl_2C_{15}N_3S_2O_{2.5}H_{24}$	$RuCl_2C_{15.7}N_3S_{2.85}O_{2.85}H_{26.1}$	$RuClF_3C_{17}N_3S_4O_6H_{27}$
Formula weight	522.47	565.84	691.17
Crystal system	Monoclinic	Orthorhombic	Triclinic
Space group	$P2_1/c$ (# 14)	*Pbca* (# 61)	$P\bar{1}$ (# 2)
Lattice parameters			
a/Å	14.169(2)	23.308(7)	18.349(4)
b/Å	10.918(2)	24.519(6)	18.869(5)
c/Å	13.689(2)	8.390(2)	7.994(1)
α/°	90	90	90.82(2)
β/°	101.77(1)	90	91.70(2)
γ/°	90	90	102.94(2)
V/Å^3	2073.0(6)	4794(2)	2695(1)
Z	4	8	4
D_{calcd}/g cm^{-3}	1.674	1.568	1.703
F_{000}	1060.00	2301.60	1400.00
μ (Mo Kα)/cm^{-1}	12.32	11.44	10.48
Independent reflection	5454	5503	12388
Data to parameter ratio	22.35	19.65	19.63
$R1$ [$I > 2\sigma(I)$]/No. of reflection	0.038/3331	0.065/2554	0.045/7221
$wR2$ (all data)	0.124/5454	0.192/5503	0.134/12388
GOF	1.15	1.55	1.20

Table 2. Selected Bond Lengths (Å) for **1**, **2**, and **3·(OTf)**

	trans[a)]	**1**	**2**	**3·(OTf)**
Ru–N bond				
	Cl		Ru(1)–N(1), 2.117(7)	Ru(1)–N(1), 2.101(4)
				Ru(2)–N(4), 2.104(4)
	S	Ru(1)–N(1), 2.131(4)	Ru(1)–N(3), 2.133(6)	Ru(1)–N(3), 2.120(4)
		Ru(1)–N(3), 2.123(4)		Ru(2)–N(6), 2.126(4)
Ru–Cl bond				
	Cl	Ru(1)–Cl(1), 2.411(1)		
		Ru(1)–Cl(2), 2.398(1)		
	S		Ru(1)–Cl(1), 2.455(2)	
	N		Ru(1)–Cl(2), 2.439(2)	Ru(1)–Cl(1), 2.399(1)
				Ru(2)–Cl(2), 2.398(1)
Ru–S bond				
	Cl		Ru(1)–S(1), 2.221(2)	
	N	Ru(1)–S(1), 2.270(1)	Ru(1)–S(2), 2.307(2)	Ru(1)–S(2), 2.299(1)
		Ru(1)–S(2), 2.283(1)		Ru(2)–S(5), 2.296(1)
	O			Ru(1)–S(1), 2.213(1)
				Ru(2)–S(4), 2.218(2)
Ru–O bond				
	S			Ru(1)–O(3), 2.175(3)
				Ru(2)–O(6), 2.171(4)
S–O bond				
in dmso-*S*	Cl		S(1)–O(1), 1.475(6)	
	N	S(1)–O(1), 1.482(4)	S(2)–O(2), 1.464(6)	S(2)–O(2), 1.480(4)
		S(2)–O(2), 1.495(4)		S(5)–O(5), 1.469(4)
	O			S(1)–O(1), 1.481(4)
				S(4)–O(4), 1.470(4)
in dmso-*O*	S			S(3)–O(3), 1.520(4)
				S(6)–O(6), 1.520(4)

a) Coordinated atom in *trans* position.

Table 3. Selected Bond Angles (°) for **1**, **2**, and **3•(OTf)**

1		**2**		**3•(OTf)**	
Axial					
Cl(1)–Ru(1)–Cl(2),	178.1(1)	Cl(1)–Ru(1)–S(1),	174.3(1)	S(1)–Ru(1)–O(3),	176.0(1)
				S(4)–Ru(2)–O(6),	176.6(1)
Axial–Equatorial					
Cl(1)–Ru(1)–N(1),	87.4(1)	Cl(1)–Ru(1)–N(1),	85.8(2)	O(3)–Ru(1)–N(1),	85.8(1)
				O(6)–Ru(2)–N(4),	87.1(2)
Cl(1)–Ru(1)–N(3),	88.5(1)	Cl(1)–Ru(1)–N(3),	86.9(2)	O(3)–Ru(1)–N(3),	87.2(1)
				O(6)–Ru(2)–N(6),	87.0(2)
Cl(1)–Ru(1)–S(1),	93.8(1)	Cl(1)–Ru(1)–Cl(2),	91.2(1)	O(3)–Ru(1)–Cl(1),	88.3(1)
				O(6)–Ru(2)–Cl(2),	88.3(1)
Cl(1)–Ru(1)–S(2),	94.3(1)	Cl(1)–Ru(1)–S(2),	87.9(1)	O(3)–Ru(1)–S(2),	86.2(1)
				O(6)–Ru(2)–S(5),	85.8(1)
Cl(2)–Ru(1)–N(1),	91.6(1)	S(1)–Ru(1)–N(1),	88.5(2)	S(1)–Ru(1)–N(1),	90.6(1)
				S(4)–Ru(2)–N(4),	89.8(1)
Cl(2)–Ru(1)–N(3),	89.8(1)	S(1)–Ru(1)–N(3),	92.5(2)	S(1)–Ru(1)–N(3),	94.3(1)
				S(4)–Ru(2)–N(6),	94.0(1)
Cl(2)–Ru(1)–S(1),	87.1(1)	S(1)–Ru(1)–Cl(2),	94.5(1)	S(1)–Ru(1)–Cl(1),	95.4(1)
				S(4)–Ru(2)–Cl(2),	94.9(1)
Cl(2)–Ru(1)–S(2),	87.3(1)	S(1)–Ru(1)–S(2),	93.3(1)	S(1)–Ru(1)–S(2),	92.4(1)
				S(4)–Ru(2)–S(5),	93.4(1)
Equatorial					
N(1)–Ru(1)–N(3),	81.1(1)	N(1)–Ru(1)–N(3),	88.3(2)	N(1)–Ru(1)–N(3),	87.0(2)
				N(4)–Ru(2)–N(6),	87.1(2)
S(1)–Ru(1)–S(2),	91.1(1)	Cl(2)–Ru(1)–S(2),	84.2(1)	Cl(1)–Ru(1)–S(2),	87.4(1)
				Cl(2)–Ru(2)–S(5),	86.8(1)
N(1)–Ru(1)–S(2),	92.8(1)	N(1)–Ru(1)–S(2),	97.4(2)	N(1)–Ru(1)–S(2),	95.1(1)
				N(4)–Ru(2)–S(5),	95.0(1)
N(3)–Ru(1)–S(1),	95.0(1)	N(3)–Ru(1)–Cl(2),	89.9(2)	N(3)–Ru(1)–Cl(1),	89.8(1)
				N(6)–Ru(2)–Cl(2),	90.4(1)
Around N atom of NH					
C(1)–N(2)–C(6),	123.9(4)	C(1)–N(2)–C(6),	131.0(7)	C(1)–N(2)–C(6),	129.2(4)
				C(17)–N(5)–C(22),	129.6(5)
Dihedral angle[a)]					
Plane(1)–Plane(2),	48.2(2)	Plane(1)–Plane(2),	25.9(3)	Plane(1)–Plane(2),	30.8(2)
				Plane(3)–Plane(4),	29.3(2)

a) Plane(1) = N(1), C(1), C(2), C(3), C(4), C(5); Plane(2) = N(3), C(6), C(7), C(8), C(9), C(10); Plane(3) = N(4), C(17), C(18), C(19), C(20), C(21); Plane(4) = N(6), C(22), C(23), C(24), C(25), C(26).

Results and Discussion

Synthesis and Characterization. As shown in Scheme 1, the reaction of *trans*-[$RuCl_2$(dmso-*S*)$_4$] with Hdpa at 273 K afforded **1** exclusively in a moderate to good yield (≈75%). In addition, spontaneous precipitation of **1** allowed for convenient collection without further purification.

The ^{1}H NMR spectrum of **1** in DMSO-d_6 had one singlet signal with an intensity of 1H in lowest field, two signals with intensities of 2H and one multiplet signal with an intensity of 4H in the aromatic region, and a broad singlet with 12H intensity in the aliphatic region (Fig. S1). It was deduced from the signal intensities that **1** possesses one Hdpa and two dmso ligands. The spectral pattern indicated that the two pyridine rings of Hdpa are equivalent; in other words, two identical ligands occupy the *trans* position to the Hdpa ligand. The spectrum suggested that two dmso ligands in *trans*-[$RuCl_2$(dmso-*S*)$_4$] were substituted by an Hdpa ligand to afford the mono(di-2-pyridylamine)ruthenium(II) complex *trans*(Cl),*cis*(S)-[$RuCl_2$(Hdpa)(dmso-*S*)$_2$], in which the *trans*(Cl)-configuration of the starting material is retained. The aromatic signals were assigned on the basis of their coupling constants[35] and H–H COSY experiments. The X-ray crystal structure showed that the geometry of **1** is in agreement with that of the *trans*(Cl),-*cis*(S)-isomer proposed based on the ^{1}H NMR spectrum.

When the thermodynamically unstable *trans*(Cl),*cis*(S)-iso-

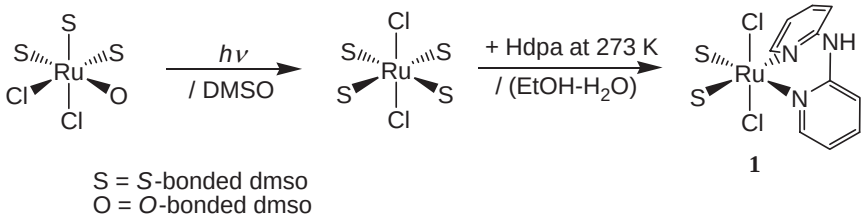

Scheme 1.

mer **1** was dissolved in DMSO, it slowly isomerized to the *cis*(Cl),*cis*(S)-isomer **2**, along with *cis*(Cl),*trans*(X)-isomer (X = *S*- or *O*-bonded dmso). This isomerization reaction is similar to that of the analogous bpy complex *trans*(Cl),-*cis*(S)-[$RuCl_2$(bpy)(dmso-*S*)$_2$].[24] Although the bpy ligand in the analogous mono(2,2′-bipyridine)ruthenium complex does not dissociate to yield free bpy ligand, the Hdpa ligand in **1** dissociated to yield free Hdpa ligand. The isomerization reaction of **1** will be discussed in detail in a later section.

The *cis*(Cl),*cis*(S)-isomer **2** was synthesized according to the synthesis method used for *cis*(Cl),*cis*(S)-[$RuCl_2$(bpy)-(dmso-*S*)$_2$].[24] The reaction of **1** in a solution of EtOH–DMSO (14:1) resulted in selective precipitation of **2**, which has a lower solubility than that of the other products. Further heating caused the conversion of **2** to the *cis*(Cl),*trans*(X)-isomer or $\mathbf{3}^+$ and the decline in the yield of **2**.

The ^{1}H NMR spectrum of **2** in DMSO-d_6 had one singlet signal with 1H in lowest field, eight signals with intensities of 1H in the aromatic region, and four aliphatic signals with intensities of 3H (Fig. S2). The spectral pattern indicated that **2** is an isomer of **1** and that the two pyridine rings of the Hdpa ligand are in different environments. Therefore, the Cl^- and dmso ligands must occupy *trans* positions to the Hdpa ligand (*cis*(Cl),*cis*(S)-isomer). The spectrum of **2** is comparable to that of *cis*(Cl),*cis*(S)-[$RuCl_2$(bpy)(dmso-*S*)$_2$].[24] The aromatic signals were assigned on the basis of their coupling constants[35] and H–H COSY experiments. An X-ray crystal structure showed that the geometry of **2** is that of the *cis*(Cl),*cis*(S)-isomer proposed based on the ^{1}H NMR spectrum.

After heating **2** to 373 K for 10 min in DMSO, one equiv of Ag(OTf) was added and AgCl precipitated quantitatively (95%). After removal of this precipitate by filtration, a yellow product, **3•(OTf)**, was obtained in good yield (83%) by precipitation. The high yield and purity of **3•(OTf)** indicated that one of the two Cl^- ligands is more labile and may selectively be substituted by solvent DMSO to yield [RuCl(Hdpa)(dmso)$_3$]-(OTf).

The ^{1}H NMR spectrum of **3•(OTf)** in DMSO-d_6 had one singlet with an intensity of 1H in lowest field, and six signals with intensities of 1H and one multiplet signal with an intensity of 2H in the aromatic region; these were assigned to the Hdpa ligand (Fig. S3). It was deduced from the spectrum that the two pyridine rings of the Hdpa ligand exist in different environments. Therefore, the Cl^- and dmso ligands occupy the *trans* position to the Hdpa ligand, that is, the equatorial Cl^- ligand in the reactant **2** is retained in the product $\mathbf{3}^+$. The aromatic signals were assigned on the basis of their coupling constants[35] and H–H COSY experiments. In the aliphatic region, six aliphatic singlets, assigned to the methyl groups of the three coordinated dmso ligands, were observed. The singlets

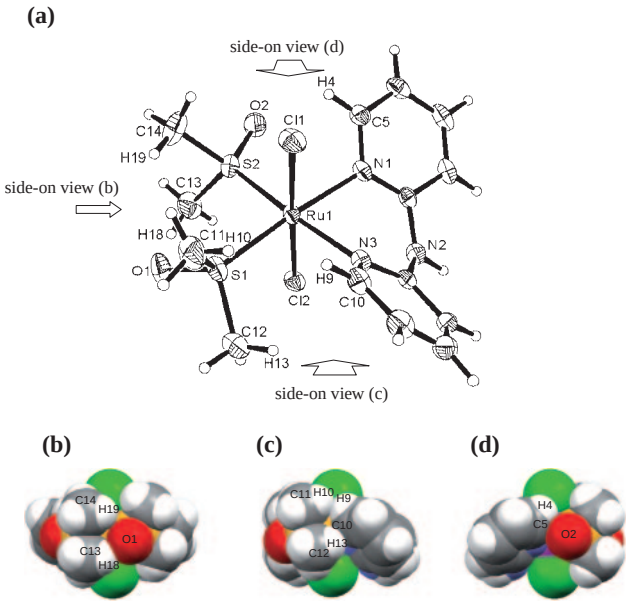

Fig. 1. (a) ORTEP drawing of **1•0.5EtOH** with 30% probability ellipsoids. The ethanol molecule is omitted for clarity. (b) Space-filling model, side-on view of **1** showing the interaction between the two dmso-*S* ligands. (c) Space-filling model, side-on view of **1** showing the interaction between Hdpa and dmso-S(1) ligands. (d) Space-filling model, side-on view of **1** showing the interaction between Hdpa and dmso-S(2) ligands.

at 3.40 and 3.08 ppm with intensities of 3H corresponded to one dmso ligand. Although the intensities of remaining four singlets at 2.61, 2.68, 2.72, and 3.36 ppm were 2H, the four singlets were assigned to two dmso ligands. A total of 4H deficiency in the intensities of the four signals (2H instead of 3H) corresponded to a 4H intensity of the signal of free DMSO. Therefore, these results indicate that the axial Cl^- ligand of **2** was substituted by a dmso ligand to afford **3•(OTf)**, which has *mer*(dmso)-configuration, and $\mathbf{3}^+$ has one inert and two labile dmso ligands. The lability of the dmso ligand in $\mathbf{3}^+$ is discussed in more detail in a later section.

Crystal Structures. *trans*(Cl),*cis*(S)-[$RuCl_2$(Hdpa)-(dmso-*S*)$_2$]•0.5EtOH (1•0.5EtOH): An ORTEP drawing of **1•0.5EtOH** is shown in Fig. 1a. The Ru ion had a distorted octahedral geometry with two *trans*(Cl) atoms (*trans*(Cl),-*cis*(S)-isomer). The Ru–Cl and Ru–S distances in **1** were similar to the corresponding distances in the analogous bpy complex *trans*(Cl),*cis*(S)-[$RuCl_2$(bpy)(dmso-*S*)$_2$].[24]

The most interesting feature of the structure of **1** was found in the Hdpa ligand. Hdpa acts as a bidentate ligand through its

two pyridine nitrogen atoms N(1) and N(3). The Ru–N distances (2.131(4) and 2.123(4) Å) were slightly longer than those of *cis*(Cl),*cis*(CO)-[$RuCl_2$(Hdpa)$(CO)_2$] (2.107(3) Å), which has sterically small co-ligands (Cl and CO). In other words, the Hdpa ligand is subject to a strong *trans* influence from CO and little steric effect from the neighboring *cis* co-ligand.[36] Therefore, the longer Ru–N distance in **1** was attributed to the steric effect of *cis* dmso ligands within the equatorial plane rather than to the *trans* influence of the dmso ligand. Moreover, the chelate ring conformation of the Hdpa ligand is greatly influenced by steric effects. The six-membered chelate ring Ru(1)–N(1)–C(1)–N(2)–C(6)–N(3) adopted a boat conformation, with the Ru(1) and N(2) atoms 0.970 and 0.357 Å, respectively, below the plane defined by the remaining four atoms. The bottom of the boat-shaped ring in **1** was deeper than that of *cis*(Cl),*cis*(CO)-[$RuCl_2$(Hdpa)$(CO)_2$], in which the chelate ring adopts a boat conformation with corresponding displacements 0.772 and 0.365 Å. The individual pyridine rings in the Hdpa ligand had a dihedral angle of 48.2(2)°, and the N(1)–Ru(1)–N(3) bite angle was 81.1(1)°. These angles indicated that the shape of the Hdpa ligand in **1** is due to repulsive interactions from the two dmso ligands within the equatorial plane; in other words, the steric effects within the equatorial plane in **1** are greater than those in *cis*(Cl),*cis*(CO)-[$RuCl_2$(Hdpa)$(CO)_2$] with a corresponding dihedral angle of 35.56° and a bite angle of 86.0(2)°.[36]

Another interesting feature of the structure of **1** is the conformation of the equatorial dmso ligands. The conformation of dmso ligands in *trans*-[$RuCl_2$(dmso-*S*)$_4$] and *trans*(Cl),*cis*(S)-[$RuCl_2$(bpy)(dmso-*S*)$_2$] have been described as engaged gearwheels.[25,26] In these complexes, the O atom of one dmso ligand is positioned between two methyl groups of another dmso ligand. Space-filling models of **1** with side-on view are shown in Figs. 1b to 1d. As shown in Fig. 1b, the O(1) atom of the dmso-S(1) ligand was not positioned between two methyl groups of the dmso-S(2) ligand; the dmso-S(1) ligand was rotated around the Ru(1)–S(1) bond to achieve contact between the O(1) atom and the H(18) atom of the methyl-C(13) group (O(1)···H(18) distance = 2.219 Å). As shown in Fig. 1c, the C(10)–H(9) moiety (6′-position) of the Hdpa ligand was in contact with two methyl groups of the dmso-S(1) ligand: the H(10) atom of methyl-C(11) group and the H(13) atom of the methyl-C(12) group. The H(9)···H(10) distance (2.113 Å) and H(13)···C(10) distance (2.544 Å) were shorter than the expected H···H and H···C distances based on van der Waals radii (2.2 and 2.88 Å, respectively).[42] Repulsive interaction caused the dmso-S(1) ligand to rotate around the Ru(1)–S(1) bond and the pyridine-N(3) ring to be pushed in the direction of the bend in the Hdpa ligand. On the other side, as shown in Fig. 1d, there was a similar repulsive interaction between the O(2) atom of the dmso-S(2) ligand and the C(5)–H(4) moiety (6-position) of the Hdpa ligand. The H(4)···O(2) distance (2.424 Å) and the O(2)···C(5) distance (2.792 Å) were shorter than the expected H···O and O···C distances based on van der Waals radii (2.68 and 3.35 Å, respectively).[42] The O(2) atom approached the side of the C(5)–H(4) moiety to make an O(2)···H(4)–C(5) angle of 102.7°, and the interaction between O(2) and the C(5)–H(4) moiety is repulsive. The repulsive interaction caused the pyridine-N(1) ring to be pushed in the direction of the bend in the Hdpa ligand. Although the repulsive interaction should cause rotation of the dmso-S(2) ligand around the Ru(1)–S(2) bond, the O(1) atom of the dmso-S(1) ligand stops the dmso-S(2) ligand from rotating. Therefore, the two dmso-*S* ligands can be thought of as engaged gearwheels that swivel in opposite directions and come to a standstill, and they push the two pyridine rings into more bent conformation of the Hdpa ligand. In other words, the conformations of the Hdpa and two dmso-*S* ligands within the equatorial plane are determined by intramolecular steric interactions with each other. Moreover, the repulsive interactions decrease the thermodynamic stability of **1** in comparison to that of **2**.

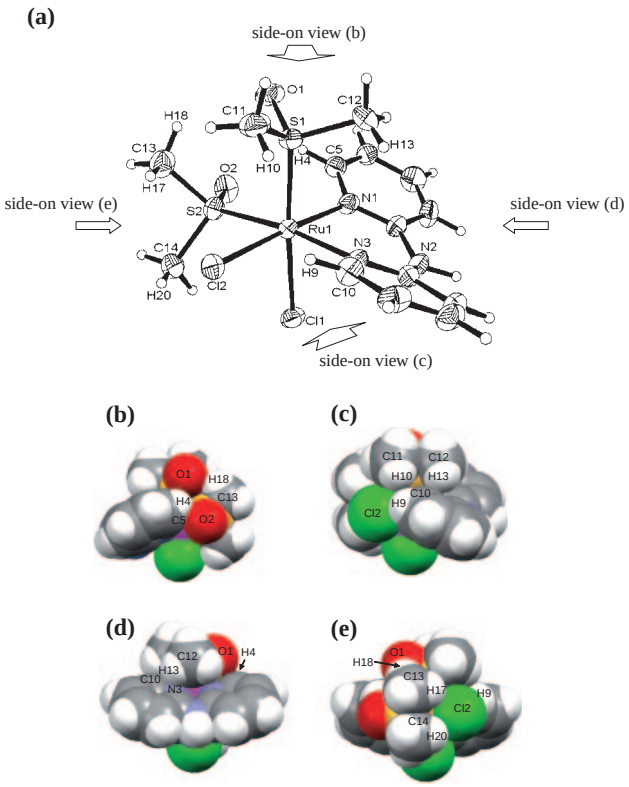

Fig. 2. (a) ORTEP drawing of **2•0.85DMSO** with 30% probability ellipsoids. The DMSO molecule is omitted for clarity. (b) Space-filling model, side-on view of **2** showing the interaction between the two dmso-*S* ligands and Hdpa. (c) Space-filling model, side-on view of **2** showing the interaction between Hdpa and Cl(1) or axial dmso-S(1) ligands. (d) Space-filling model, side-on view of **2** showing the interaction between Hdpa and axial dmso-S(1) ligands. (e) Space-filling model, side-on view of **2** showing the interaction between dmso-S(2) and Cl(2) ligands within the equatorial plane.

***cis*(Cl),*cis*(S)-[$RuCl_2$(Hdpa)(dmso-*S*)$_2$]•0.85DMSO (2•0.85DMSO):** An ORTEP drawing of **2•0.85DMSO** is shown in Fig. 2a. The Ru ion had a distorted octahedral geometry with the Cl atom *trans* to the S atom of the dmso ligand (*cis*(Cl),*cis*(S)-isomer). The Ru–Cl and Ru–S distances in **2** were similar to the corresponding distances in the analogous bpy complex *cis*(Cl),*cis*(S)-[$RuCl_2$(bpy)(dmso-*S*)$_2$].[24]

The Cl(2) and S(2) were in the equatorial positions and *trans* to the Hdpa ligand. The Ru(1)–Cl(2) and Ru(1)–S(2)

distances (2.439(2) and 2.307(2) Å, respectively) were significantly longer than the corresponding distances in **1** (av. 2.405 and av. 2.277 Å, respectively). The longer bonds suggested that the steric interactions among Cl(2), dmso-S(2), and Hdpa ligands in the equatorial plane are significant. The greater N(1)–Ru(1)–S(2) angle (97.4(2)°) and the smaller Cl(2)–Ru(1)–S(2) angle (84.2(1)°) compared to **1** also suggested that there are steric effects between the equatorial ligands.

The Ru–N distances in **2** (2.117(7) and 2.133(6) Å) were similar to those of **1** (av. 2.127 Å). However, the chelate ring conformation of the Hdpa ligand in **2** was different from that of **1**. The six-membered chelate ring Ru(1)–N(1)–C(1)–N(2)–C(6)–N(3) adopted a boat conformation, with the Ru(1) and N(2) atoms 0.552 and 0.222 Å, respectively, below the plane defined by the remaining four atoms. The bottom of the boat-shaped ring in **2** was shallower than that of **1**, in which the corresponding atoms were 0.970 and 0.357 Å below the plane. The individual pyridine rings in the Hdpa ligand had a dihedral angle of 25.9(3)°, which was smaller than that of **1** (48.2(2)°), and the N(1)–Ru(1)–N(3) bite angle of 88.3(2)° was closer to the ideal angle (90°) in the octahedral geometry than that of **1** (81.1(1)°). These angles of **2** indicated that the steric effect within the equatorial plane in **2** is smaller than that of **1**, which contains two bulky *S*-bonded dmso ligands within the equatorial plane.

The interesting features of the structure of **2** are the interactions between the crowded ligands. As shown in Fig. 2b, the H(4) atom in the pyridine-N(1) ring of the Hdpa ligand was pinched by the O(1) atom of the axial dmso-S(1) ligand and the O(2) atom of the equatorial dmso-S(2). The H(4)···O(1) distance (2.684 Å) was similar to the expected H···O distance based on van der Waals radii (2.68 Å).[42] The H(4)···O(2) distance (2.237 Å) and C(5)···O(2) distance (2.892 Å) were shorter than the expected H···O and O···C distances based on van der Waals radii (2.68 and 3.35 Å, respectively).[42] The O(2) atom approached the side of the C(5)–H(4) moiety to make an O(2)···H(4)–C(5) angle of 125.3°, and there was repulsion between the C(5)–H(4) moiety on the pyridine-N(1) ring and O(2) atom of the equatorial dmso-S(2) ligand. As shown in Fig. 2c, for the other pyridine ring of the Hdpa ligand, the C(10)–H(9) moiety (6′-position) of the Hdpa ligand was in contact with the H(13) atom of the methyl-C(12) group of the axial dmso-S(1) ligand, and the equatorial Cl(2) atom. The H(13)···C(10) distance (2.900 Å) was similar to the expected H···C distance based on van der Waals radii (2.88 Å), and the C(10)···Cl(2) distance (3.159 Å) was shorter than the expected C···Cl distance based on van der Waals radii (3.54 Å).[42] Consequently, as shown in Fig. 2d, the axial dmso-S(1) ligand flattened the Hdpa ligand towards a more shallow conformation, while the equatorial dmso-S(2) and Cl(2) ligands pushed the Hdpa ligand towards a more bent conformation.

As shown in Fig. 2e, in addition to the Cl(2)···H(9) interaction, two C–H···Cl hydrogen-bonding interactions were observed between the Cl(2) and the two methyl groups of the equatorial dmso ligands. The H(17)···Cl(2) distance (2.826 Å) and the H(20)···Cl(2) distance (2.681 Å) were shorter than the expected H···Cl distances based on van der Waals radii (2.86 Å).[42] The O(1) atom of the axial dmso-S(1) ligand was also hydrogen-bonded to the H(18) atom of the methyl-C(13) group of the equatorial dmso-S(2) ligand (2.395 Å).

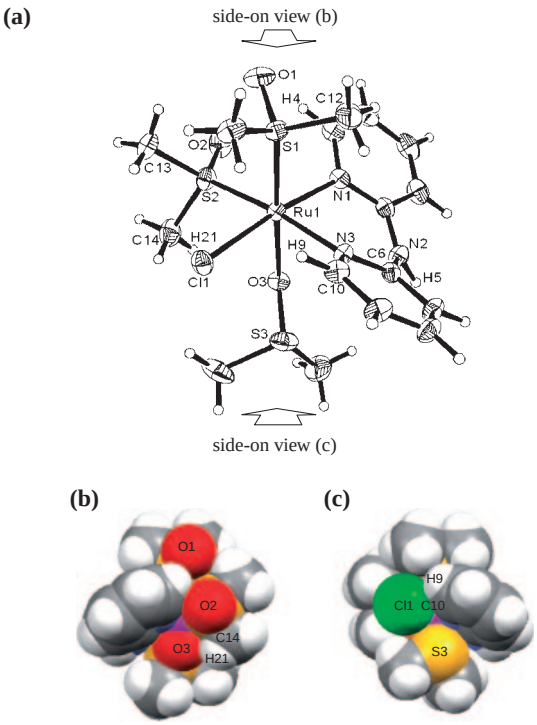

Fig. 3. (a) ORTEP drawing of the Ru(1) cation (one of two crystallographically independent cations) of **3·(OTf)** with 30% probability ellipsoids. The OTf^- anion is omitted for clarity. (b) Space-filling model, side-on view of $\mathbf{3}^+$ showing the interaction between the three dmso ligands, and between Hdpa and the two dmso-*S* ligands. (b) Space-filling model, side-on view of $\mathbf{3}^+$ showing the interaction between equatorial dmso-S(1) and axial dmso-O(3) ligands. (c) Space-filling model, side-on view of $\mathbf{3}^+$ showing the interaction between axial dmso-O(3) and Cl(1) ligands.

***cis*(Cl,S),*trans*(O,S)-[RuCl(Hdpa)(dmso-*O*)(dmso-*S*)$_2$]-(OTf) (3·(OTf)):** The crystal structure of **3·(OTf)** showed that the asymmetric unit contained two crystallographically independent complex cations, Ru(1) and Ru(2), and two crystallographically independent counter-anions, OTf-S(7) and OTf-S(8). The structures of complex cations Ru(1) and Ru(2) were quite similar. The structure of cation, Ru(1) is shown in Fig. 3a. The Ru cations had slightly distorted octahedral geometries, with the S atom of one dmso ligand *trans* to the O atom of another dmso ligand and *cis* to the S atom of a third dmso ligand (*mer*(dmso)-configuration). The amino groups of the Hdpa ligands faced towards the dmso-O(3) or the dmso-O(6) ligands.

The structural parameters and the conformations of the two dmso-*S*, chloro, and Hdpa ligands in $\mathbf{3}^+$ (apart from the dmso-*O* ligand) were essentially the same as those of **2**, except for the axial Cl^- ligand. The remaining axial site was occupied by the *O*-donor of the dmso ligand instead of the *S*-donor. We have previously reported the structure of *cis*(Cl),*trans*(S)-[$RuCl_2$(bpy)(dmso-*S*)$_2$], which has two *S*-bonded dmso ligands in the *trans* position; *O*-coordination of the dmso ligand requires not only *trans* influence but also steric effects.[24] The Ru–O bond distances (av. 2.173 Å) were slightly longer than

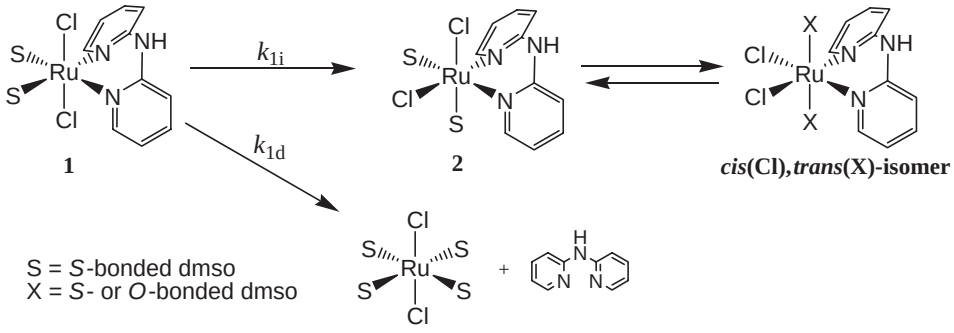

Scheme 2.

those of *cis*(Cl),*fac*(S)-[$RuCl_2$(dmso-*S*)$_3$(dmso-*O*)] (2.134(3) Å)[25] and *cis*(Cl),*cis*(S),*cis*(O)-[$RuCl_2$(dmso-*S*)$_2$(dmso-*O*)(CO)] (2.123(2) Å),[43] in which the O atoms are *trans* to the *S*-bonded dmso ligands. The elongation of the axial Ru–O bond suggested that the axial *O*-bonded dmso ligands are subject to a steric repulsive interaction from the equatorial dmso ligands. As shown in Fig. 3b, the distances between the O atoms of the axial *O*-bonded dmso ligands and the methyl-C atoms of the equatorial dmso ligands (av. 3.016 Å) were shorter than the expected C···O distance based on van der Waals radii (3.35 Å).[42] The axial O atoms slightly contacted the methyl groups of the equatorial dmso ligands. Therefore, the *S*-donor of the dmso ligand, which is larger than the O and the Cl atoms, is unable to enter the axial coordination site (van der Waals radii: O, 1.58 Å; Cl, 1.76 Å; and S, 1.81 Å).[42]

The most interesting feature of the structure of $\mathbf{3}^+$ was the structure of the *O*-bonded dmso ligand. The S–O bond distances of *O*-bonded dmso ligands (av. 1.520 Å) were longer than those of *S*-bonded dmso ligands (1.469(4)–1.481(4) Å). The electronic structure of sulfoxides may be represented by a resonance hybrid of these structures:[44]

$$\text{>}S^+\text{—}O^- \rightleftharpoons \text{>}S{=}O \qquad (1)$$

If coordination occurs through the O atom, the contribution of the S^+–O^- structure increases, resulting in elongation of the S–O bond. Therefore, the slightly positive charge on the S atom of the axial dmso-*O* ligand restricts its own conformation. As shown in Fig. 3c, the S(3) atom of the axial dmso-*O* ligand faced towards the Cl(1) ligand. The distances between the S atoms of the *O*-bonded dmso ligands and the equatorial Cl ligands (av. 3.418 Å) were shorter than the expected S···Cl distance based on van der Waals radii (3.57 Å),[42] and the S^+ atoms interacted with the Cl^- ligands by electrostatic attraction to restrict rotation of the axial dmso-*O* ligand around the O–S bond.

Although the bite angles of the Hdpa ligands (av. 87.1°) in **3•(OTf)** were similar to that observed in **2** (88.3(2)°), the dihedral angles of the two pyridyl rings of the Hdpa ligands (av. 30.1°) were significantly larger than that of **2** (25.9(3)°). The chelate ring conformation of the Hdpa ligands in $\mathbf{3}^+$ was also different from that of **2**. The six-membered chelate rings adopted boat conformations, with the Ru and bridgehead N atoms av. 0.720 and av. 0.279 Å, respectively, below the plane defined by the remaining four atoms (Table S2). The bottom of the boat conformation in $\mathbf{3}^+$ was deeper than that in **2** (with distances below the plane of 0.552 and 0.222 Å), but similar to that in *cis*(Cl),*cis*(CO)-[$RuCl_2$(Hdpa)$(CO)_2$] (0.772 and 0.365 Å), in which there was little steric effect from the neighboring *cis* co-ligand.[36] This difference in the chelate ring conformation of the Hdpa ligands was caused by the difference in van der Waals radii of the axial-coordinated atoms, O (1.58 Å) in $\mathbf{3}^+$ and Cl (1.76 Å) in **2**.[42] In $\mathbf{3}^+$, because the axial coordination site was occupied by the smaller O atom of the dmso-*O* ligand, which resulted in extra room around the axial O atom, the conformations of the Hdpa ligands, which were flattened from the opposite direction by the axial dmso-*S* ligands, are able to change. The S_{axial}–Ru–N angles (av. 92.2°) were larger than corresponding angles in **2** (av. 90.5°). This indicated that the N atoms of the Hdpa ligands tilt towards the axial O atom and the bottom of boat-shaped ring at the Ru atom side becomes deeper. The transformation of the Hdpa ligand causes relaxation of the repulsive interactions of the Hdpa ligand with the equatorial dmso and Cl^- ligands. In the Ru(1) cation case, the O(2) atom of the equatorial dmso ligand was in contact with the C(5)–H(4) moiety (6-position) of the pyridine-N(1) ring. The O(2) atom approached the C(5)–H(4) moiety from the side to make an O(2)···H(4)–C(5) angle of 114.1°, and the interaction between O(2) and the C(5)–H(4) moiety is repulsive. Although the C(5)···O(2) distance (2.874 Å) was similar to the C(5)···O(2) distance in **2** (2.892 Å), the H(4)···O(2) distance (2.352 Å) was longer than the H(4)···O(2) distance in **2** (2.237 Å), and the repulsive interaction in $\mathbf{3}^+$ was less than in **2**. In the other pyridine ring (pyridine-N(3)), the C(10)···Cl(1) distance (3.200 Å) is greater than the C(10)···Cl(2) distance in **2** (3.159 Å). Therefore, the repulsive interactions among the atoms of the equatorial plane in the Ru(1) cation are smaller than those in **2**. The situation of the Ru(2) cation is also similar to that of the Ru(1) cation.

Isomerization Reaction of 1 in DMSO Solution. The isomerization reaction of *trans*(Cl),*cis*(S)-isomer **1** in DMSO solution is summarized in Scheme 2. A DMSO-d_6 solution of **1** was sealed in an NMR tube and heated at 323 K, and the isomerization reaction was monitored over a 3 h period by means of NMR spectroscopy. The ^{1}H NMR spectrum of the solution after 1 h of heating is shown in Fig. 4, along with the ^{1}H NMR spectra of *trans*(Cl),*cis*(S)-isomer **1** and free Hdpa; extra signals in addition to the signals of *trans*(Cl),*cis*(S)-isomer **1** were observed. Some of the extra signals were assigned to free Hdpa and *cis*(Cl),*cis*(S)-isomer **2** by comparison with the spectra of authentic samples. As shown in Fig. 4b, the H-3, H-4, and H-5 signals of free Hdpa and *cis*(Cl),*cis*(S)-isomer **2** overlapped,

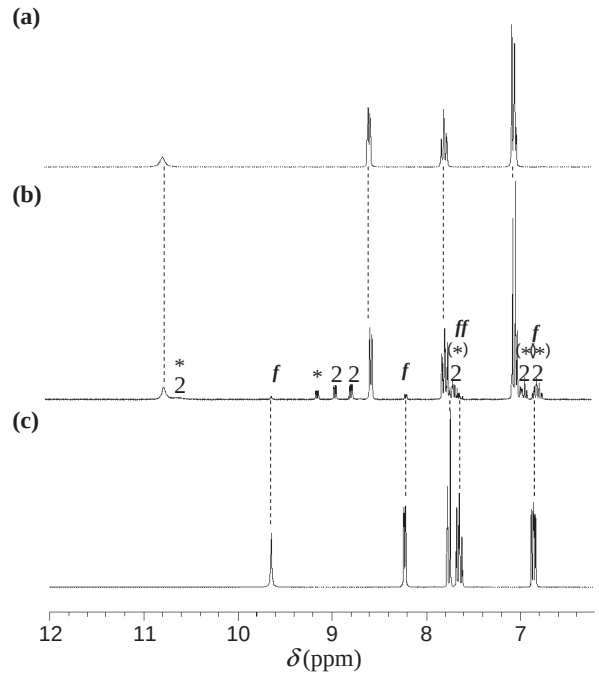

Fig. 4. ^{1}H NMR spectra of **1** in DMSO-d_6: (a) immediately after dissolution; (b) after 1 h of heating at 323 K. (c) ^{1}H NMR spectrum of free Hdpa in DMSO-d_6. ^{1}H NMR spectra were recorded at room temperature (≈298 K). Signals marked with asterisks are the signals of *cis*(Cl),-*trans*(X)-[$RuCl_2$(Hdpa)(dmso)$_2$].

but the five H-6 signals at 8.0–9.2 ppm were independent and were assigned. Only one signal at 9.14 ppm (d, $J = 6.2$ Hz, H-6) could not be assigned by reference to authentic samples. The sum of the intensity of the five H-6 signals was constant during the reaction, and the species with one H-6 signal at 9.14 ppm was the only one formed. Although the species could not be isolated, a single H-6 signal indicated that the two pyridine rings of the Hdpa ligand are equivalent. Therefore, the species is probably the third isomer *cis*(Cl),*trans*(X)-[$RuCl_2$-(Hdpa)(dmso)$_2$] (X = *S*- or *O*-bonded dmso), which is analogous to the mono(2,2′-bipyridine)ruthenium complex.[24] The coordination atoms (S or O) of the dmso ligands were unknown; therefore, a crystal structure for the *cis*(Cl),*trans*(X)-isomer is desirable.

The reaction rate for the isomerization of *trans*(Cl),*cis*(S)-isomer **1** to *cis*(Cl),*cis*(S)-isomer **2** was determined by ^{1}H NMR spectroscopy in DMSO-d_6 at 323 K. As the reaction proceeds, the signal of *trans*(Cl),*cis*(S)-isomer **1** decreased, and the signals of *cis*(Cl),*cis*(S)-isomer **2** and free Hdpa increased. The decrease in the peak intensity of the H-6 proton signal of *trans*(Cl),*cis*(S)-isomer **1** (intensities were normalized with respect to a reference signal of mesitylene) was plotted over two half-lives and was found to obey simple first-order decay kinetics with a rate constant ($k_{obs} = k_{1i} + k_{1d}$) of $(1.32 \pm 0.01) \times 10^{-4}$ s^{-1} ($t_{1/2} = 87 \pm 1$ min). This indicated that the reverse reaction to regenerate *trans*(Cl),*cis*(S)-isomer **1** is very slow and is negligible compared to the isomerization reaction of *trans*(Cl),*cis*(S)-isomer **1**, i.e., the isomerization reaction between *trans*(Cl),*cis*(S)-isomer **1** and *cis*(Cl),*cis*(S)-isomer **2** is irreversible. The ratio of the increase in peak intensity of the H-6 proton signal of the free Hdpa to the decease in the corresponding peak intensity in of *trans*(Cl),*cis*(S)-isomer **1** was found to be constant (0.12) over two half-lives. Therefore, the dissociation rate constant (k_{1d}) was $(0.16 \pm 0.01) \times 10^{-4}$ s^{-1}, and the isomerization rate constant (k_{1i}) was $(1.16 \pm 0.01) \times 10^{-4}$ s^{-1}. The value of k_{1i} at 323 K was smaller than that of the analogous mono(2,2′-bipyridine)ruthenium complex *trans*(Cl),*cis*(S)-[$RuCl_2$(bpy)(dmso-*S*)$_2$] ($k = (4.0 \pm 0.1) \times 10^{-4}$ s^{-1},$t_{1/2} = 29 \pm 1$ min).[24]

The *trans*(Cl),*cis*(S)-isomer **1** had a coplanar equatorial mean plane (within ±0.018 Å), as defined by N(1), N(3), S(1), and S(2), in which the Ru atom is displaced from this plane towards the Cl(1) atom by 0.043 Å. In contrast, the analogous bpy complex *trans*(Cl),*cis*(S)-[$RuCl_2$(bpy)(dmso-*S*)$_2$] has a significantly distorted coplanar equatorial mean plane (within ±0.128 Å). The large distortion is caused by significant steric interactions between the two dmso-*S* and the bpy ligands, which forms a rigid five-membered chelate ring with the Ru ion. The good planarity of the equatorial mean plane in **1** suggests that the flexible six-membered chelate ring formed by the Hdpa ligand with the Ru ion takes on all of the steric hindrance in the equatorial plane. Furthermore, the flexible six-membered chelate ring in **1** causes the smaller value of k_{1i} for **1** than that for the analogous bpy complex.

The value of k_{1i} and k_{1d} were determined at four temperatures in the range 303–333 K (Fig. S4), and the activation parameters of the isomerization and dissociation were calculated: for the isomerization $\Delta H^{\ddagger} = 133 \pm 2$ kJ mol^{-1} and $\Delta S^{\ddagger} = 90 \pm 7$ J mol^{-1} K^{-1}, and for the dissociation $\Delta H^{\ddagger} = 123 \pm 2$ kJ mol^{-1} and $\Delta S^{\ddagger} = 42 \pm 4$ J mol^{-1} K^{-1}. The activation parameters for the isomerization were similar to those for the *trans* to *cis* thermal isomerization of *trans*-[$RuCl_2$(dmso-*S*)$_4$] ($\Delta H^{\ddagger} = 128 \pm 2$ kJ mol^{-1} and $\Delta S^{\ddagger} = 110 \pm 5$ J mol^{-1} K^{-1}).[25] Therefore, the large $\Delta H^{\ddagger}$ and positive $\Delta S^{\ddagger}$ values suggested a dissociative mechanism for the isomerization similar to that of *trans*-[$RuCl_2$(dmso-*S*)$_4$], in which the rate-determinating step is the release of a dmso ligand from **1**. For the dissociation, the $\Delta S^{\ddagger}$ value was positive but smaller than those for the isomerization. The large $\Delta H^{\ddagger}$ and smaller positive $\Delta S^{\ddagger}$ values suggested that the dissociation proceeded probably through an intermediate with a monodentate Hdpa ligand.

The ratio of the increase in peak intensity of the H-6 proton signal of *cis*(Cl),*cis*(S)-isomer **2** to the decease in the corresponding peak intensity of *trans*(Cl),*cis*(S)-isomer **1** was found not to be constant (0.88) and decreased as time passed. This suggested that *cis*(Cl),*cis*(S)-isomer **2** undergoes a further reaction, i.e., the isomerization reaction to the *cis*(Cl),*trans*(X)-isomer.

Isomerization Reaction of 2 in DMSO Solution. When dissolved in DMSO, *cis*(Cl),*cis*(S)-isomer **2** isomerized to the *cis*(Cl),*trans*(X)-isomer and the *cis*(Cl,S),*trans*(O,S)-[RuCl-(Hdpa)(dmso-*O*)(dmso-*S*)$_2$]$^+$ (Scheme 3). This isomerization reaction was similar to that of the analogous bpy complex *cis*(Cl),*cis*(S)-[$RuCl_2$(bpy)(dmso-*S*)$_2$].[24]

The reaction rate for the isomerization reaction of *cis*(Cl),-*cis*(S)-isomer **2** was determined by ^{1}H NMR spectroscopy in DMSO-d_6 at 303 K, since the reaction rate of **2** at 323 K was too fast to allow the time course of the reaction to be followed. A DMSO-d_6 solution of *cis*(Cl),*cis*(S)-isomer **2**, with mesity-

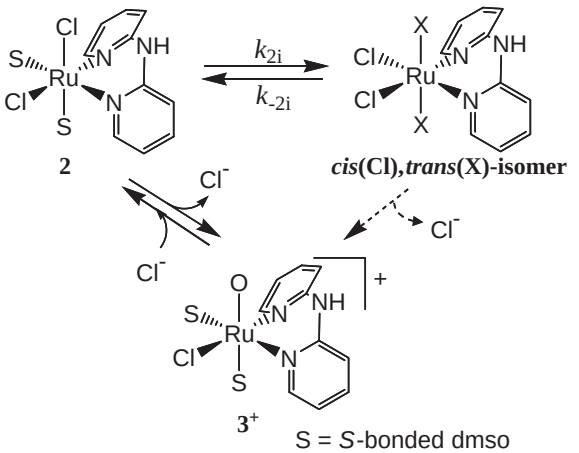

Scheme 3.

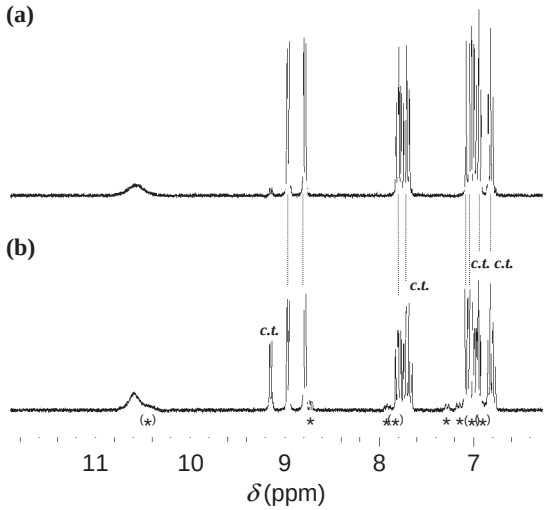

Fig. 5. ^{1}H NMR spectra of **2** in DMSO-d_6: (a) immediately after dissolution; (b) after 10 h of heating at 303 K. ^{1}H NMR spectra were recorded at room temperature (≈298 K). Signals marked with "*c.t.*" are signals of *cis*(Cl),*trans*(X)-[$RuCl_2$(Hdpa)(dmso)$_2$], and those with asterisks are signals of $\mathbf{3}^+$.

lene as an internal reference, was sealed in an NMR tube and heated to 303 K, and the isomerization reaction was monitored over a 10 h period by means of NMR spectroscopy. As the reaction proceeded, the signals of *cis*(Cl),*cis*(S)-isomer **2** decreased, and signals of *cis*(Cl),*trans*(X)-isomer increased. The ^{1}H NMR spectrum of the solution after 10 h of heating is shown in Fig. 5. Extra signals in addition to the nine signals of *cis*(Cl),*cis*(S)-isomer **2** were observed. The additional signal at 9.14 ppm (d, $J = 6.2$ Hz, H-6) was assigned to the *cis*(Cl),-*trans*(X)-isomer. The signals for H-3, H-4, and H-5 of the *cis*(Cl),*trans*(X)-isomer were obscured by the signals of *cis*(Cl),*cis*(S)-isomer **2**. The remaining small signals, which are labeled with asterisks in Fig. 5, were assigned to $\mathbf{3}^+$ by comparison with the spectrum of an authentic sample. During isomerization of *cis*(Cl),*cis*(S)-isomer **2** to *cis*(Cl),*trans*(X)-isomer, signals due to *trans*(Cl),*cis*(S)-isomer **1** were not observed. These results indicated that the isomerization reaction

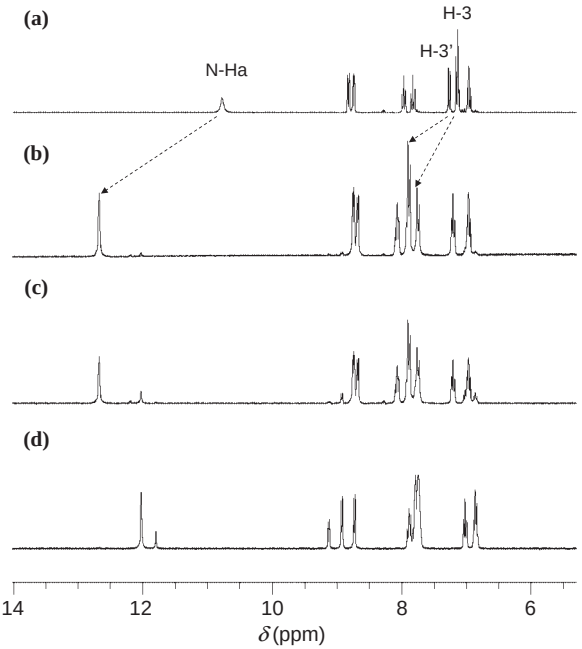

Fig. 6. ^{1}H NMR spectra of **3•(OTf)** with ca. 100 equiv of LiCl in DMSO-d_6: (a) **3•(OTf)** only; (b) after dissolution (5 min at 303 K); (c) after 0.5 h at 303 K; (d) after 16 h at 303 K. ^{1}H NMR spectra were recorded at 303 K.

between *trans*(Cl),*cis*(S)-isomer **1** and *cis*(Cl),*cis*(S)-isomer **2** is irreversible, and the isomerization reaction of *cis*(Cl),-*cis*(S)-isomer **2** yields *cis*(Cl),*trans*(X)-[$RuCl_2$(Hdpa)(dmso)$_2$] with an additional substitution reaction, in which the axial Cl^- ligand is replaced by a solvent DMSO molecule to form $\mathbf{3}^+$.

The formation reaction of $\mathbf{3}^+$ was slow in comparison to the isomerization reaction. During this time, an equilibrium was established between the *cis*(Cl),*cis*(S)-isomer **2** and the *cis*(Cl),*trans*(X)-isomer, slightly favoring **2**; $K_{23} = k_{2i}/k_{-2i} = 0.32 \pm 0.01$. If this system is treated as a reversible first-order reaction, the rate constants for the isomerizations **2** → *cis*(Cl),*trans*(X) and *cis*(Cl),*trans*(X) → **2** are calculated as $k_{2i} = (2.2 \pm 0.1) \times 10^{-5}$ s^{-1} and $k_{-2i} = (6.9 \pm 0.1) \times 10^{-5}$ s^{-1}, respectively.

The *mer*(dmso)-complex $\mathbf{3}^+$ may be afforded by substitution of the axial Cl^- ligand in **2** or one of the equatorial Cl^- ligands in the *cis*(Cl),*trans*(X)-isomer with a solvent DMSO. An attempt to determine the reaction path and rate for the formation of $\mathbf{3}^+$ using ^{1}H NMR spectroscopy was unsuccessful due to comparatively slow reaction rate.

Reaction of $\mathbf{3}^+$ with Chloride Ion. A DMSO-d_6 solution of $\mathbf{3}^+$ with ca. 100 equiv of LiCl (1.5–2.0 mol/L) was sealed in an NMR tube and then maintained at 303 K. The ^{1}H NMR spectrum of the solution is shown in Fig. 6. Figure 6b shows the shift in the spectrum of $\mathbf{3}^+$ after dissolution, which occurred immediately upon addition of Cl^- ion in DMSO solution. The signals of the N-Ha and H-3 protons were shifted downfield by significant amounts (N-Ha; 1.90 ppm, H-3; 0.62 ppm), while the signals of the H-4, H-5, and H-6 protons slightly shifted (H-4; 0.09 ppm, H-5; 0.04 ppm, and H-6; −0.08 ppm). These shifts indicate that the Cl^- ion is associated with the N-Ha proton of the Hdpa ligand in $\mathbf{3}^+$ through hydrogen bonding. Figure 6c shows the reaction at $t = 30$ min. A

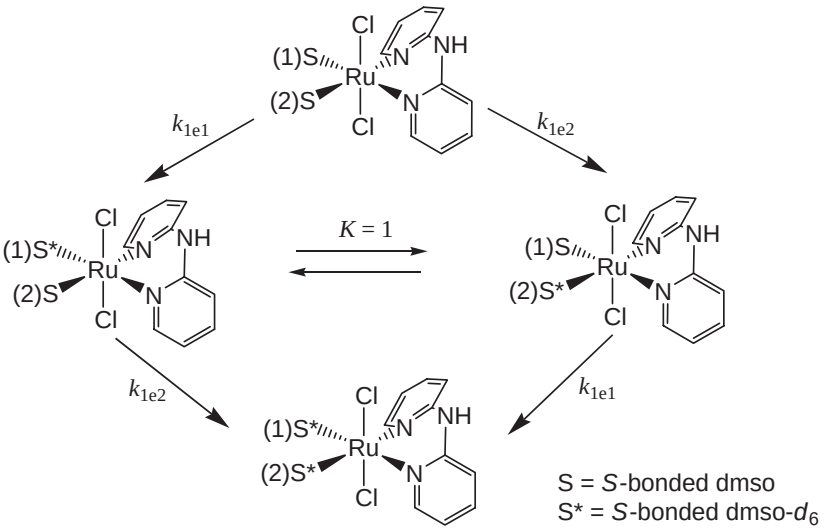

Scheme 4.

signal due to *cis*(Cl),*cis*(S)-isomer **2** appeared (8.93 ppm, d, H-6), but signals due to the *cis*(Cl),*trans*(X)-isomer were scarcely observed. This suggested that the axial *O*-bonded dmso ligand in $\mathbf{3}^+$ is substituted by a Cl^- ion to yield *cis*(Cl),*cis*(S)-isomer **2**. In Fig. 6d, which shows the reaction at $t = 16$ h, the signals of $\mathbf{3}^+$ had completely disappeared, and signals of *cis*(Cl),-*cis*(S)-isomer **2** and the *cis*(Cl),*trans*(X)-isomer were observed.

The decrease in the peak intensity of the H-6 proton signal of $\mathbf{3}^+$ in the presence of a large excess of Cl^-, normalized with respect to the mesitylene reference signal, was plotted over two half-lives. It was found to obey pseudo-first-order decay kinetics, with a rate constant (k_3) of $(10.1 \pm 0.1) \times 10^{-5}\ s^{-1}$ ($t_{1/2} = 115 \pm 2$ min). At the initial stage of the reaction (30 min), the *cis*(Cl),*cis*(S)-isomer **2** was the dominant product; the ratio [*cis*(Cl),*trans*(X)]/[*cis*(Cl),*cis*(S)-**2**] was 0.08. The ratio increased as time passed, reaching 0.21 at 240 min. It is suggested that the reaction of $\mathbf{3}^+$ with Cl^- affords *cis*(Cl),-*cis*(S)-isomer **2**, and the isomerization reaction to the *cis*(Cl),-*trans*(X)-isomer follows.

Conformation and Solvent Exchange Reaction of dmso Ligands in DMSO Solution. ***trans*(Cl),*cis*(S)-Isomer 1:** According to the crystal structure of *trans*(Cl),*cis*(S)-isomer **1**, the conformations of Hdpa and the two dmso ligands cause the four methyl groups to be in different environments. If the conformations of the Hdpa and dmso ligands are maintained in solution, and hence comparable to those in the crystal, four methyl signals should be observable in ^{1}H NMR spectrum. In DMSO-d_6 solution, however, the four methyl groups of *trans*(Cl),*cis*(S)-isomer **1** were observed as a broad singlet on the ^{1}H NMR timescale (3.15 ppm). Therefore, it is suggested that the Hdpa ligand is "flapping" and the two dmso ligands rotate around the Ru–S bonds, giving rise to time-averaged C_{2v} symmetry.

A solution of *trans*(Cl),*cis*(S)-isomer **1** in DMSO-d_6 was sealed in an NMR tube and kept at 303 K. In the resulting ^{1}H NMR spectrum after 2 h, some isomerization of *trans*(Cl),-*cis*(S)-isomer **1** to *cis*(Cl),*cis*(S)-isomer **2** and decomposition of **1** was observed, but 93% of the original amount of **1** remained. The methyl signal at 3.15 ppm, however, had decreased to 68.5% of its intensity in the initial spectrum. Therefore, the solvent exchange reaction of dmso ligands is faster than the isomerization reaction of **1** to **2**. On the basis of the decay in intensity of the methyl signal over two half-lives, $k_{obs} = (0.48 \pm 0.01) \times 10^{-4}\ s^{-1}$ ($t_{1/2} = 241 \pm 3$ min). The rate constant of the isomerization and decomposition reaction ($k_{1i} + k_{1d}$), on the basis of the decay in intensity of the H-6 signals of **1** during the initial reaction until 70% of **1** remained, was $(0.05 \pm 0.01) \times 10^{-4}\ s^{-1}$. Thus, the inherent exchange reaction of dmso ligands has a rate constant of $k_{obs\text{-}1e} = k_{obs} - (k_{1i} + k_{1d}) = (0.43 \pm 0.01) \times 10^{-4}\ s^{-1}$.

The two dmso ligands in **1** may exchange at different rates; the exchange process is a set of stepwise reactions as shown in Scheme 4.[45] The species having only one dmso* (dmso* = dmso-d_6) ligand are in equilibrium ($K = 1$) with a quick conversion because of the absence of isotope effects. According to the rate law,[46] $k_{obs\text{-}1e} = 1/2(k_{1e1} + k_{1e2})$, i.e., it is the average of the rate constants of exchange reaction of dmso-S(1) and -S(2). However, the Ru(1)–S(1) distance (2.270(1) Å) was similar to the Ru(1)–S(2) distance (2.283(1) Å), and so the difference between k_{1e1} and k_{1e2} is small. Therefore, the exchange reaction of **1** may be discussed using the average of the rate constants $1/2(k_{1e1} + k_{1e2})$ and the structural parameters of the dmso-S(2) ligand.

***cis*(Cl),*cis*(S)-Isomer 2:** In DMSO solution, the four methyl groups (two dmso ligands) of the *cis*(Cl),*cis*(S)-isomer **2** were not equivalent on the ^{1}H NMR time-scale (2.66, 3.25, 3.26, and 3.35 ppm); in other words, the rotation of the two dmso ligands around the Ru–S bonds is restricted even in DMSO solution. The intramolecular hydrogen bonds deduced from the crystal structure should also be evident in DMSO solution. This feature has been found in the analogue bpy complex *cis*(Cl),*cis*(S)-[$RuCl_2$(bpy)(dmso-*S*)$_2$].[24]

A solution of *cis*(Cl),*cis*(S)-isomer **2** in DMSO-d_6 was sealed in an NMR tube and kept at 303 K. In the resulting ^{1}H NMR spectrum after 2 h, some *cis*(Cl),*trans*(X)-isomer had been formed (15%) with 85% of *cis*(Cl),*cis*(S)-isomer **2** remaining. The two dmso ligands have very different rates of solvent exchange. The intensities of the methyl signals at

2.66 and 3.25 ppm were 75% of their intensities in initial spectrum. The decay rate constant (k_{obs1}) was $(0.27 \pm 0.01) \times 10^{-4}\,s^{-1}$ ($t_{1/2} = 436 \pm 7$ min), which is similar to k_{2i} ($(0.22 \pm 0.01) \times 10^{-4}\,s^{-1}$). Therefore, the decrease in the intensity of the signals at 2.66 and 3.25 ppm was caused mainly by isomerization of **2** to the *cis*(Cl),*trans*(X)-isomer, and the rate constant for the inherent exchange of the dmso ligands was small ($k_{obs1\text{-}2i} = (k_{obs1} - k_{2i}) = (0.05 \pm 0.01) \times 10^{-4}\,s^{-1}$). In contrast, the intensities of the two remaining methyl signals (3.26 and 3.35 ppm) were 40% of those in the initial spectrum; only 50% of the surviving **2** molecules retained the original dmso ligands without solvent exchange. The decrease in the intensity of the signals is caused by isomerization of **2** to the *cis*(Cl),*trans*(X)-isomer and inherent solvent exchange in **2**. The decay rate constant (k_{obs2}) was $(1.13 \pm 0.01) \times 10^{-4}\,s^{-1}$ ($t_{1/2} = 103 \pm 1$ min), which is greater than k_{2i} ($(0.22 \pm 0.01) \times 10^{-4}\,s^{-1}$). Thus, the inherent solvent exchange of the dmso ligands with signals at 3.26 and 3.35 ppm had a rate constant of $k_{obs2\text{-}2i} = (k_{obs2} - k_{2i}) = (0.91 \pm 0.01) \times 10^{-4}\,s^{-1}$. This meant that the solvent exchange reaction of one of the two dmso ligands of *cis*(Cl),*cis*(S)-isomer **2** is slower than that of the other by a factor of 100; in other words, the dmso ligand with methyl signals at 2.66 and 3.25 ppm is inert, while the one with methyl signals at 3.26 and 3.35 ppm is labile.

The equatorial and axial dmso ligands were distinguished spectroscopically by assigning the methyl signals on the basis of the ring-current effect. The chemical shift of one methyl signal (2.66 ppm) was a significant distance from those of the others (3.25, 3.26, and 3.35 ppm). The methyl-C(12) group was situated above the pyridine-N(3) ring of the Hdpa ligand and was subject to the ring-current effect of the pyridine-N(3) ring. Therefore, the signals at 2.66 and 3.25 ppm were assigned to the protons of the methyl-C(12) and methyl-C(11) groups of the axial dmso-S(1) ligand, respectively, and the signals at 3.26 and 3.35 ppm to the methyl groups of the equatorial dmso-S(2) ligand. In other words, the inert ligand was the axial dmso-S(1) ligand ($k_{2e1} = k_{obs1\text{-}2i} = 0.05 \times 10^{-4}\,s^{-1}$), and the labile one was the equatorial dmso-S(2) ligand ($k_{2e2} = k_{obs2\text{-}2i} = (0.91 \pm 0.01) \times 10^{-4}\,s^{-1}$). In the crystal structure of *cis*(Cl),*cis*(S)-isomer **2**, the equatorial Ru(1)–S(2) bond distance (2.307(2) Å) was longer than the axial Ru(1)–S(1) bond distance (2.221(2) Å), which may mean that the axial dmso-S(1) ligand is more inert than the equatorial dmso-S(2) ligand.

The inertness of the axial dmso ligand in DMSO solution suggests that the Hdpa ligand of *cis*(Cl),*cis*(S)-isomer **2** does not flap, and the conformation of Hdpa is restricted. If the Hdpa ligand did flap, and another conformer with the reverse conformation to the Hdpa ligand existed, the situation of the axial dmso ligand would be similar to that of the axial *O*-bonded dmso ligand in $\mathbf{3}^+$, with the result that the axial dmso ligand would coordinate through the O atom; since *O*-bonded dmso ligands are labile in general,[25,26,43] the axial dmso ligand of the other conformer should be labile. This is not consistent with the evidence that the axial dmso ligand in *cis*(Cl),*cis*(S)-isomer **2** is inert. Therefore, the Hdpa ligand of *cis*(Cl),*cis*(S)-isomer **2** is fixed and does not flap, and no other conformer exists.

***mer*-(dmso)Complex 3•(OTf):** In the ^{1}H NMR spectrum of **3•(OTf)** in DMSO-d_6, the six methyl groups of the three dmso ligands were independently observed on the ^{1}H NMR time-scale (2.61, 2.68, 2.72, 3.08, 3.36, and 3.40 ppm); therefore, the rotation of the two dmso-*S* ligands around the Ru–S bonds and of the dmso-*O* ligand around the O–S bond are restricted in DMSO solution. These observations are similar to those for *cis*(Cl),*cis*(S)-isomer **2**, and the intramolecular interactions deduced from the crystal structure should also be evident in DMSO solution.

If the structure of $\mathbf{3}^+$ in solution were comparable to that of the crystal, the *O*-bonded dmso ligand should be most labile of the three dmso ligands. A DMSO-d_6 solution of **3•(OTf)** was sealed in an NMR tube and maintained at 303 K. In the ^{1}H NMR spectrum of the resulting solution after 4 min, the dmso methyl signals at 3.08 and 3.40 ppm were observed with same intensity as those in the initial spectrum, but the four remaining methyl signals at 2.61, 2.68, 2.72, and 3.36 ppm decreased to 45% of their original intensities due to exchange with the solvent DMSO-d_6. After 1 h, the methyl signals at 3.08 and 3.40 ppm showed 90% of their intensities in the initial spectrum, but the signals at 2.61, 2.68, 2.72, and 3.36 ppm had completely disappeared. The exchange occurred with $k_{obs1} = (14.6 \pm 0.4) \times 10^{-4}\,s^{-1}$ ($t_{1/2} = 7.9 \pm 0.2$ min). In contrast, the solvent exchange reaction for the dmso ligand with methyl signals at 3.08 and 3.40 ppm, on the basis of the decay in the intensities of the signals over one half-lives (8 h), occurred with $k_{obs2} = (0.24 \pm 0.01) \times 10^{-4}\,s^{-1}$ ($t_{1/2} = 477 \pm 2$ min), which is similar (on the order of 10^{-5}) to that of the equatorial dmso ligands in **1**. It can be seen that in the $\mathbf{3}^+$ complex, the exchange reaction of the two dmso ligands with methyl signals at 2.61, 2.68, 2.72, and 3.36 ppm is much faster than that of the third dmso ligand. Contrary to expectations, the former two ligands are very labile.

The two methyl signals (3.08 and 3.40 ppm) of the inert dmso ligand were assigned to the equatorial dmso ligand ($k_{3e2} = k_{obs2} = (0.24 \pm 0.01) \times 10^{-4}\,s^{-1}$), because the chemical shifts were similar to those of the equatorial dmso ligand in *trans*(Cl),*cis*(S)-isomer **1** (3.15 ppm) and *cis*(Cl),*cis*(S)-isomer **2** (3.26 and 3.35 ppm). The remaining four methyl signals (2.61, 2.68, 2.72, and 3.36 ppm) of the two labile dmso ligands were assigned to the axial dmso ligands ($k_{3e1} = k_{obs1} = (14.6 \pm 0.4) \times 10^{-4}\,s^{-1}$).

Both axial dmso ligands are labile and have the same exchange rate in spite of their different coordination modes (*S*- and *O*-bonded), which suggests that mutual alternation of coordination modes occurs. This may be due to flapping of the Hdpa ligand. If the conformation of the Hdpa ligand becomes inverted without any change in the coordination modes of the two axial dmso ligands, there should be a difference in energy between the two conformers due to the difference in the interaction of Hdpa with the *O*-bonded and *S*-bonded ligands. However, if the conformation of the Hdpa ligand becomes inverted, followed by alternation of the coordination modes of the two axial dmso ligands, the resulting conformer is the same as the original. Consequently, the flapping of the Hdpa ligand must be linked to mutual changes in the coordination modes of the two axial dmso ligands, which causes high lability as both axial ligands can be considered to be *O*-bonded ligands. However, because the two axial dmso ligands are observed independently in the ^{1}H NMR spectrum of $\mathbf{3}^+$, the inversion reac-

Table 4. Kinetic Data for Exchange Reactions of dmso Ligand and Contact Distances between Equatorial dmso and Hdpa Ligands for **1**, **2**, and **3•(OTf)**

	1	**2**	**3•(OTf)**
Equatorial dmso ligands			
$k_e/10^{-4}\ s^{-1}$	0.43 ± 0.01	0.91 ± 0.01	0.24 ± 0.01
Ru–S distance/Å	2.270(1), 2.283(1)	2.307(2)	2.299(1), 2.296(1)
$(dmso)_{eq}$–Hdpa contact distance/Å	2.608[a)]	2.565[a)]	2.613[a)], 2.639[b)]
Axial dmso ligands			
$k_e/10^{-4}\ s^{-1}$	—	0.05 ± 0.01	14.6 ± 0.4
Ru–S distance/Å	—	2.221(2)	2.213(1), 2.218(2)

a) Mean of O(2)···H(4) and O(2)···C(5) distances. b) Mean of O(5)···H(31) and O(5)···C(21) distances.

tion rate must be rather slow compared to the ^{1}H NMR timescale.

Comparison of Solvent Exchange Reactions of dmso Ligands in 1, 2, and 3$^+$. The kinetic data for the exchange reactions are summarized in Table 4, along with the contact distances of equatorial dmso and Hdpa. The rate constant for solvent exchange of the equatorial dmso ligands in **2** was conspicuously larger than those of **1** and **3**$^+$, although the Ru–S distances in **2** and **3**$^+$ were nearly equivalent (2.296–2.307 Å). The repulsive interaction between the equatorial dmso ligand and the Hdpa ligand causes acceleration of the exchange reaction of equatorial dmso ligand. These repulsive interactions may be evaluated by means of the contact distance between the O atom of the equatorial dmso ligand and the C–H moiety in the 6-position of the Hdpa pyridine ring, which is the mean of the O(2)···H(4) and O(2)···C(5) distances. The contact distance of the dmso and Hdpa ligands in **2** (2.565 Å) was remarkably short compared to those of **1** (2.608 Å) and in **3**$^+$ (2.613 and 2.639 Å). This indicated that the equatorial dmso ligand in **2** is subject to stronger repulsion from Hdpa ligand than those of the other complexes and so becomes more labile than the other equatorial dmso ligands.

The axial dmso ligand in **2** is inert, while that of **3**$^+$ is just the opposite. The inertness of the ligand in **2** is reasonable because of the short Ru–S distance (2.221(2) Å). However, although the axial dmso-*S* ligand in **3**$^+$ is expected to be inert according to the Ru–S distance (2.213(1) and 2.218(2) Å), the axial dmso-*S* ligand was observed to be as labile as the axial dmso-*O* ligand. It is notable that the mutual alternation between axial dmso-*S* and dmso-*O* ligands appears to activate the inert dmso-*S* ligand.

Summary

Selective syntheses of the *trans*(Cl),*cis*(S)- and *cis*(Cl),-*cis*(S)-isomers of $[RuCl_2(Hdpa)(dmso\text{-}S)_2]$ (**1** and **2**, respectively) were carried out, and their crystal structures were reported. Our synthetic method for mono(polypyridyl)ruthenium complexes was found to be suitable for use with the type of ligand that forms a six-membered chelate ring. Although the *cis*(Cl),*trans*(X)-isomer (X = *S*- or *O*-bonded dmso) was not isolated independently, its existence was verified by means of ^{1}H NMR spectroscopy. Furthermore, the synthesis and X-ray crystal structure of *cis*(Cl,S),*trans*(S,O)-[RuCl(Hdpa)-(dmso-*O*)(dmso-*S*)$_2$](OTf) (**3•(OTf)**) were also reported.

The crystal structures of **1**, **2**, and **3•(OTf)** revealed that the conformation of the six-membered chelate ring formed by the Hdpa ligand with the Ru ion varies depending on its interactions with the co-ligands (dmso and Cl$^-$) or counter-anion (OTf$^-$). In *trans*(Cl),*cis*(S)-isomer **1**, the repulsive interactions between the C–H moieties of the 6- and 6′-positions of the Hdpa ligand and the two dmso-*S* ligands within the equatorial plane caused the pyridine rings to be pushed in the direction the bend in the Hdpa ligand. In *cis*(Cl),*cis*(S)-isomer **2**, the equatorial monodentate ligands, dmso-*S* and Cl$^-$, pushed the pyridine rings in the direction of the bend in the Hdpa ligand, and the axial dmso-*S* ligand squashes the Hdpa ligand to a flatter conformation. In **3•(OTf)**, the structural parameters were essentially the same as those of *cis*(Cl),*cis*(S)-isomer **2**, except for those of the dmso-*O* ligand (**3•(OTf)**) and the axial Cl$^-$ ligand (**2**). The remaining axial site was occupied by the *O*-donor of the dmso ligand instead of *S*-donor. The axial dmso-*O* ligand interacted with the equatorial Cl$^-$ ligand by an electrostatic attraction.

All three isomers of $[RuCl_2(Hdpa)(dmso)_2]$ underwent isomerization in DMSO solution. Isomerization from *trans*(Cl),-*cis*(S)-isomer **1** to *cis*(Cl),*cis*(S)-isomer **2** was irreversible, and *cis*(Cl),*cis*(S)-isomer **2** slowly isomerized to the *cis*(Cl),-*trans*(X)-isomer and to **3**$^+$. These isomerization reactions in DMSO solution were analogous to those of the bpy complexes $[RuCl_2(bpy)(dmso\text{-}S)_2]$.[24] The axial *O*-bonded dmso ligand in **3**$^+$ was easily substituted by Cl$^-$ ions to yield *cis*(Cl),*cis*(S)-isomer **2**.

The ^{1}H NMR spectral features of **1**, **2**, and **3•(OTf)** in DMSO-d_6 suggested that each mono(di-2-pyridylamine)ruthenium complex displays a variation of the conformation and flapping characteristics of the Hdpa ligand in DMSO solution. In *trans*(Cl),*cis*(S)-isomer **1**, the Hdpa ligand flaps and the two dmso ligands rotate around the Ru–S bonds, giving rise to a time-averaged C_{2v} symmetry. In **3•(OTf)**, the Hdpa ligand also flaps, which causes the coordination modes of the two axial dmso ligands to alternate mutually between *O*- and *S*-bonded modes. The rate of the inversion reaction was slow compared to the ^{1}H NMR timescale. The mutual alternation between axial dmso-*S* and dmso-*O* ligands appears to activate the inert dmso-*S* ligand and two axial dmso ligands became labile. In contrast, in *cis*(Cl),*cis*(S)-isomer **2**, the Hdpa ligand is fixed and not flapping, and the structure of **2** is restricted in DMSO solution.

The structures and isomerization reactions in DMSO solution of these mono(di-2-pyridylamine)ruthenium complexes were similar to those of the analogous mono(2,2′-bipyridine)-ruthenium complexes. The most interesting feature of the mono(di-2-pyridylamine)ruthenium complexes was the conformation and flapping of the flexible six-membered chelate ring of the Hdpa ligand. Experiments to explore the applicability of these complexes as new precursors for bis- or tris-heteroleptic ruthenium complexes are currently underway.

This work was financially supported by Research Project Grant (B) of the Institute of Science and Technology, Meiji University.

Supporting Information

The ^{1}H NMR spectra of **1**, **2**, **3•(OTf)**, and the plots of $\ln(k/T)$ vs $(1/T)$ for the isomerization of **1** to **2** (k_{1i}) and the dissociation of **1** (k_{1d}) are in PDF format (Figs. S1, S2, S3, and S4, respectively). The selected non-bonding contacts and angles, and the distances of Ru atom or N atom of the NH group below the plane defined by four atoms (N, C, C, N) are also in PDF format (Tables S1 and S2, respectively). This material is available free of charge on the web at http://www.csj.jp/journal/bcsj/.

References

1 A. Juris, V. Balzani, F. Barigelletti, S. Campagna, P. Belser, A. von Zelewsky, *Coord. Chem. Rev.* **1988**, *84*, 85.

2 V. Balzani, A. Juris, M. Venturi, S. Campagna, S. Serroni, *Chem. Rev.* **1996**, *96*, 759.

3 F. Barigelletti, L. Flamigni, *Chem. Soc. Rev.* **2000**, *29*, 1.

4 T. J. Meyer, *Pure Appl. Chem.* **1986**, *58*, 1193.

5 M. K. Nazeeruddin, C. Klein, P. Liska, M. Grätzel, *Coord. Chem. Rev.* **2005**, *249*, 1460.

6 M. Grätzel, *Coord. Chem. Rev.* **1991**, *111*, 167.

7 S. Ito, P. Liska, P. Comte, R. Charvet, P. Péchy, U. Bach, L. Schmidt-Mende, S. M. Zakeeruddin, A. Kay, M. K. Nazeeruddin, M. Grätzel, *Chem. Commun.* **2005**, 4351.

8 C. R. Rice, M. D. Ward, M. K. Nazeeruddin, M. Grätzel, *New J. Chem.* **2000**, *24*, 651.

9 F. Liu, G. J. Meyer, *Inorg. Chem.* **2005**, *44*, 9305.

10 Y.-Y. Lü, L.-H. Gao, M.-J. Han, K.-Z. Wang, *Eur. J. Inorg. Chem.* **2006**, 430.

11 L. Spiccia, G. B. Deacon, C. M. Kepert, *Coord. Chem. Rev.* **2004**, *248*, 1329.

12 C. M. Kepert, G. B. Deacon, N. Sahely, L. Spiccia, G. D. Fallon, B. W. Skelton, A. H. White, *Inorg. Chem.* **2004**, *43*, 2818.

13 C. M. Kepert, A. M. Bond, G. B. Deacon, L. Spiccia, B. W. Skelton, A. H. White, *Dalton Trans.* **2004**, 1766.

14 P. A. Anderson, G. B. Deacon, K. H. Haarmann, F. R. Keene, T. J. Meyer, D. A. Reitsma, B. W. Skelton, G. F. Strouse, N. C. Thomas, J. A. Treadway, A. H. White, *Inorg. Chem.* **1995**, *34*, 6145.

15 J. A. Treadway, T. J. Meyer, *Inorg. Chem.* **1999**, *38*, 2267.

16 B. T. Patterson, F. R. Keene, *Inorg. Chem.* **1998**, *37*, 645.

17 S. M. Zakeeruddin, M. K. Nazeeruddin, R. Humphry-Baker, M. Grätzel, V. Shklover, *Inorg. Chem.* **1998**, *37*, 5251.

18 G. F. Strouse, P. A. Anderson, J. R. Schoonover, T. J. Meyer, F. R. Keene, *Inorg. Chem.* **1992**, *31*, 3004.

19 H. B. Ross, M. Boldaji, D. P. Rillema, C. B. Blanton, R. P. White, *Inorg. Chem.* **1989**, *28*, 1013.

20 A. von Zelewsky, G. Gremaud, *Helv. Chim. Acta* **1988**, *71*, 1108.

21 D. A. Freedman, J. K. Evju, M. K. Pomije, K. R. Mann, *Inorg. Chem.* **2001**, *40*, 5711.

22 I. P. Evans, A. Spencer, G. Wilkinson, *J. Chem. Soc., Dalton Trans.* **1973**, 204.

23 T. Suzuki, T. Kuchiyama, S. Kishi, S. Kaizaki, H. D. Takagi, M. Kato, *Inorg. Chem.* **2003**, *42*, 785.

24 M. Toyama, K. Inoue, S. Iwamatsu, N. Nagao, *Bull. Chem. Soc. Jpn.* **2006**, *79*, 1525.

25 E. Alessio, G. Mestroni, G. Nardin, W. M. Attia, M. Calligaris, G. Sava, S. Zorzet, *Inorg. Chem.* **1988**, *27*, 4099.

26 E. Alessio, *Chem. Rev.* **2004**, *104*, 4203.

27 W. L. Huang, D. P. Segers, M. K. DeArmond, *J. Phys. Chem.* **1981**, *85*, 2080.

28 K.-Y. Ho, W.-Y. Yu, K.-K. Cheung, C.-M. Che, *J. Chem. Soc., Dalton Trans.* **1999**, 1581.

29 R. Lescouëzec, G. Marinescu, M. C. Muñoz, D. Luneau, M. Andruh, F. Lloret, J. Faus, M. Julve, J. A. Mata, R. Llusar, J. Cano, *New J. Chem.* **2001**, *25*, 1224.

30 H. Kumagai, S. Kitagawa, M. Maekawa, S. Kawata, H. Kiso, M. Munakata, *J. Chem. Soc., Dalton Trans.* **2002**, 2390.

31 S. Youngme, G. A. van Albada, N. Chaichit, P. Gunnasoot, P. Kongsaeree, I. Mutikainen, O. Roubeau, J. Reedijk, U. Turpeinen, *Inorg. Chim. Acta* **2003**, *353*, 119.

32 M. Burgos, O. Crespo, M. C. Gimeno, P. G. Jones, A. Laguna, *Eur. J. Inorg. Chem.* **2003**, 2170.

33 T. Fukuchi, N. Nagao, E. Miki, K. Mizumachi, T. Ishimori, *Bull. Chem. Soc. Jpn.* **1989**, *62*, 2076.

34 N. Nagao, M. Mukaida, E. Miki, K. Mizumachi, T. Ishimori, *Bull. Chem. Soc. Jpn.* **1994**, *67*, 2447.

35 N. Nagao, M. Mukaida, S. Tachiyashiki, K. Mizumachi, *Bull. Chem. Soc. Jpn.* **1994**, *67*, 1802.

36 M. Haukka, P. D. Costa, S. Luukkanen, *Organometallics* **2003**, *22*, 5137.

37 M. Ishaq, A. O. Baghlaf, M. I. Al-Khatery, Y. Al-Anquary, *J. Chem. Soc. Pak.* **1993**, *15*, 36.

38 A. O. Baghlaf, K. Banaser, H. Y. Hashem, A. Ali Bishry, M. Ishaq, *Qatar Univ. Sci. J.* **1994**, *14*, 75.

39 N. C. Thomas, G. B. Deacon, *Synth. React. Inorg. Met.-Org. Chem.* **1986**, *16*, 85.

40 E. Steinhäuser, E. Diepolder, *J. Prakt. Chem.* **1916**, *93*, 387.

41 *teXsan Crystal Structure Analysis Package*, Molecular Structure Corporation, **1992**.

42 R. S. Rowland, R. Taylor, *J. Phys. Chem.* **1996**, *100*, 7384.

43 E. Alessio, E. Iengo, S. Geremia, M. Calligaris, *Inorg. Chim. Acta* **2003**, *344*, 183.

44 N. Nakamoto, *Infrared and Raman Spectra of Inorganic and Coordination Compounds, Part B: Applications in Coordination, Organometallic, and Bioinorganic Chemistry*, 5th ed., Wiley-Interscience, John Wiley & Sons, Inc., **1997**, p. 102.

45 W. G. Jackson, A. F. M. M. Rahman, M. A. Wong, *Inorg. Chim. Acta* **2004**, *357*, 665.

46 In the reaction scheme for the solvent exchange reaction of **1**, [$RuCl_2$(Hdpa)(dmso-S(1))(dmso-S(2))], **A**; [$RuCl_2$(Hdpa)-(dmso*-S(1))(dmso-S(2))], **B1**; [$RuCl_2$(Hdpa)(dmso-S(1))(dmso*-S(2))], **B2**; [$RuCl_2$(Hdpa)(dmso*-S(1))(dmso*-S(2))], **C**; the rate of the disappearance of **A** and the formation of **B1** + **B2** is given by the following equations: $d[\mathbf{A}]/dt = -(k_{1e1} + k_{1e2})[\mathbf{A}]$ (1) and $d[\mathbf{B1} + \mathbf{B2}]/dt = (k_{1e1} + k_{1e2})[\mathbf{A}] - k_{1e2}[\mathbf{B1}] - k_{1e1}[\mathbf{B2}]$ (2).

When $K = 1$ and so $[\mathbf{B1}] = [\mathbf{B2}]$, $d[\mathbf{B1} + \mathbf{B2}]/dt = (k_{1e1} + k_{1e2})[\mathbf{A}] - 1/2(k_{1e1} + k_{1e2})[\mathbf{B1} + \mathbf{B2}]$ (3). Thus, integrating Eq. 1 and Eq. 3 give: $[\mathbf{A}] = [\mathbf{A}]_0 e^{-(k1e1+k1e2)t}$ (4) and $[\mathbf{B1} + \mathbf{B2}] = 2[\mathbf{A}]_0(e^{-1/2(k1e1+k1e2)t} - e^{-(k1e1+k1e2)t})$ (5), respectively, where $[\mathbf{A}]_0$ is initial concentration of **A** at $t = 0$. The coordinated dmso signal in the ^{1}H NMR spectrum is proportional to $2[\mathbf{A}] + [\mathbf{B1} + \mathbf{B2}]$ with proportionality constant ε. Using peak heights as a measure of area, $H_t = \varepsilon(2[\mathbf{A}] + [\mathbf{B1} + \mathbf{B2}]) = \varepsilon(2[\mathbf{A}]_0 e^{-1/2(ke1+ke2)t})$ (6), $H_{t\infty} = 0$, and $H_{t0} = \varepsilon(2[\mathbf{A}]_0)$. Thus, $H_t/H_{t0} = e^{-1/2(k1e1+k1e2)t}$ (7). Therefore, the observed rate constant $k_{\text{obs-1e}} = 1/2(k_{1e1} + k_{1e2})$ (8).